

Impact of Neutral Density on the Magnetic Shielding of Hall Thrusters

IEPC-2019-276

*Presented at the 36th International Electric Propulsion Conference
University of Vienna, Austria
September 15–20, 2019*

Sarah E. Cusson,^{*} Benjamin A. Jorns[†] and Alec D. Gallimore[‡]
University of Michigan, Ann Arbor, MI 48109

The ion velocity distribution functions in the near-wall region of a 9-kW magnetically shielded Hall thruster, the H9, and a 33-kW two-channel magnetically shielded Hall thruster, the N30, are experimentally characterized as a function of local neutral density to assess changes to ion trajectories and high energy tails. Velocity measurements are performed using laser-induced fluorescence for the H9 operating at 300 V and 15 A at 4.6 and 15.8 μ Torr-Xe and the N30 inner channel operating at 300 V and 15 A with and without the outer channel nominal flow. Mean ion velocity measurements along the channel centerline show that the main acceleration region is downstream of the exit plane of these Hall thrusters and that as the local neutral density increases, the acceleration region shifts upstream. This is consistent with previous studies on magnetically-shielded Hall thrusters. Ion velocity measurements along the H9 chamfers show that while the mean ion trajectories in the near-wall region do not change appreciably with changing neutral density, the high energy tail towards the wall does increase at high pressure, likely yielding a higher erosion rate. The N30, on the other hand, demonstrates no increase in the high-energy tail of the energy distribution. Both results suggest that a grazing line electron temperature of 7 eV would protect the walls from erosion. It is argued that this condition is satisfied for both systems. Combined, these results indicate that neutral density impacts are minimal on the magnetic shielding of Hall thrusters.

^{*}Ph.D Candidate, Department of Aerospace Engineering, cusson@umich.edu

[†]Assistant Professor, Department of Aerospace Engineering

[‡]Robert J. Vlasic Dean of Engineering, the Richard F. and Eleanor A. Towner Professor of Engineering, and Arthur F. Thurnau Professor of Aerospace Engineering

Nomenclature

e	= Elementary charge
E	= Electric field
E_1	= Secondary electron emission crossover energy
$f(u)$	= Ion velocity distribution function
k	= Boltzmann's constant
L	= Length scale
m	= Mass
n_e	= Electron density
r	= Radial position
T_e	= Electron temperature
u	= Ion velocity
z	= Axial position
γ_e	= Secondary electron emission yield
ϕ	= Plasma potential
σ_0	= Effective yield at zero energy

I. Introduction

Magnetic shielding has effectively eliminated the historical main failure mechanism for Hall thrusters, discharge chamber erosion.¹⁻⁷ The technology works by exploiting the isothermality of magnetic field lines in the thruster. By shaping the magnetic field such that the field lines adjacent to the wall reach into the near anode region, “cold” electrons extend along the entirety of the discharge chamber walls. At this low temperature, the field lines are approximately equipotential, resulting in high plasma potential along the grazing field line, comparable to the anode potential. This potential structure results in near-wall ions with low kinetic energy and a low sheath potential drop from the grazing line to the wall. Combined, these two effects lower the impact energy of ions to the wall to below that of the threshold sputtering energy of most common discharge chamber materials. This advancement in Hall thruster technology has enabled these thrusters to be viable for a wider mission realm, including deep space missions.⁶

The exact implications of this new magnetic field configuration on Hall thruster operation remains an open area of research. While the technology is an extension of current Hall thruster configurations, the subtle differences induced by shielding when compared to traditional thruster configurations are crucial to understand from both a physics and flight-risk perspective. To this end, there have been numerous studies which have investigated potential changes in performance^{1,8} and stability.⁹⁻¹¹ Overall, these studies found that for high-power thrusters ($>1\text{kW}$), the overall efficiency only decreased 1% as compared to un-shielded thrusters.¹ Additionally, they found that of the three main oscillation types typically seen in Hall thrusters (breathing mode between 1 and 20 kHz, cathode oscillations between 70 and 100 kHz, and azimuthal spokes between 10 and 40 kHz), only the breathing mode and cathode oscillations were present for magnetically shielded thrusters.^{9,10} However, this lack of azimuthal modes does not appear to impact the overall performance of the thruster. Finally, it was found that magnetically shielded thrusters have increased pole erosion^{12,13} and could react differently to facility effects when compared to their unshielded counterparts.^{11,14} Of particular importance is the latter effect: facility impacts. These are related to the known difference in the behavior of Hall

thrusters in ground test facilities versus in-space operation. These changes are often associated with differences in the neutral density environment induced by the pressure changes. While many parameters are impacted by the neutral density, the location of the bulk plasma is known to shift depending on facility pressure.^{15,16} This location, called the “acceleration region,” has broad ranging influence on other thruster parameters, such as performance and stability. However, its impact on the lifetime of the thruster, particularly for magnetically shielded thrusters, remains unknown.

In this study, we aim to investigate the impact of neutral density from two different sources on the magnetic shielding of Hall thrusters. First, we consider the facility pressure changes. Other works have measured the movement of the acceleration region with varying pressure.^{15,17} Thus, there is reason to believe the temperature of the grazing line is also changing with pressure. However, to our knowledge, there has been no investigation of ion velocities along the wall of magnetically shielded Hall thrusters to quantify facility impacts on the shielding and therefore lifetime. These potential changes to lifetime take on additional importance when we consider the next generation of Hall thrusters such as nested Hall thrusters (NHTs). NHTs are being invested in for human and cargo missions to Mars.¹⁸ These thrusters concentrically nest multiple discharges together and can be operated in single- or multi-channel mode. However, in multi-channel operation, adjacent channels act as significant neutral sources. Indeed, previous studies have shown shifts in the location of the acceleration region depending on firing configuration.¹⁹ Therefore, neutrals from adjacent channels could impact the grazing line temperature of magnetically shielded NHTs, ultimately impacting the overall lifetime of these devices. This comprises our second source for neutral impacts on magnetically shielded Hall thrusters.

The goal of this work is to understand the impact neutral changes have on the magnetic shielding of Hall thrusters. In order to accomplish this goal, we organize the paper as follows: we begin with a discussion of magnetic shielding theory, specifically focusing on how neutrals could impact this theory. We then present our experimental apparatus, followed by the results from the facility pressure study. Next, we show the results from the NHT study. Finally, we discuss the implications of our results and make concluding remarks.

II. Theory

In principle, magnetic shielding works by exploiting two fundamental properties of Hall thrusters: (1) the isothermality of magnetic force lines and (2) the magnetic-force-line equipotentialization at low electron temperatures. Mathematically, the first principle can be expressed as

$$\nabla_{\parallel} T_e \approx 0, \quad (1)$$

where T_e is the electron temperature and ∇_{\parallel} is the gradient parallel to the magnetic field. The second principle stems from the Boltzmann relation:

$$\phi \approx \phi_0 + T_{e0} \log \frac{n_e}{n_{e0}}, \quad (2)$$

where ϕ is the plasma potential and n_e is the plasma density. The subscript 0 indicates an integration constant. Equation 2 yields a critical component to magnetic shielding in that the induced parallel electric field is,

$$E_{\parallel} = -T_e \nabla_{\parallel} \log n_e. \quad (3)$$

The first equation arises from the thermal transport of electrons along magnetic force lines resulting in rapid equilibrium and constant electron temperature along the line. The second equation implies

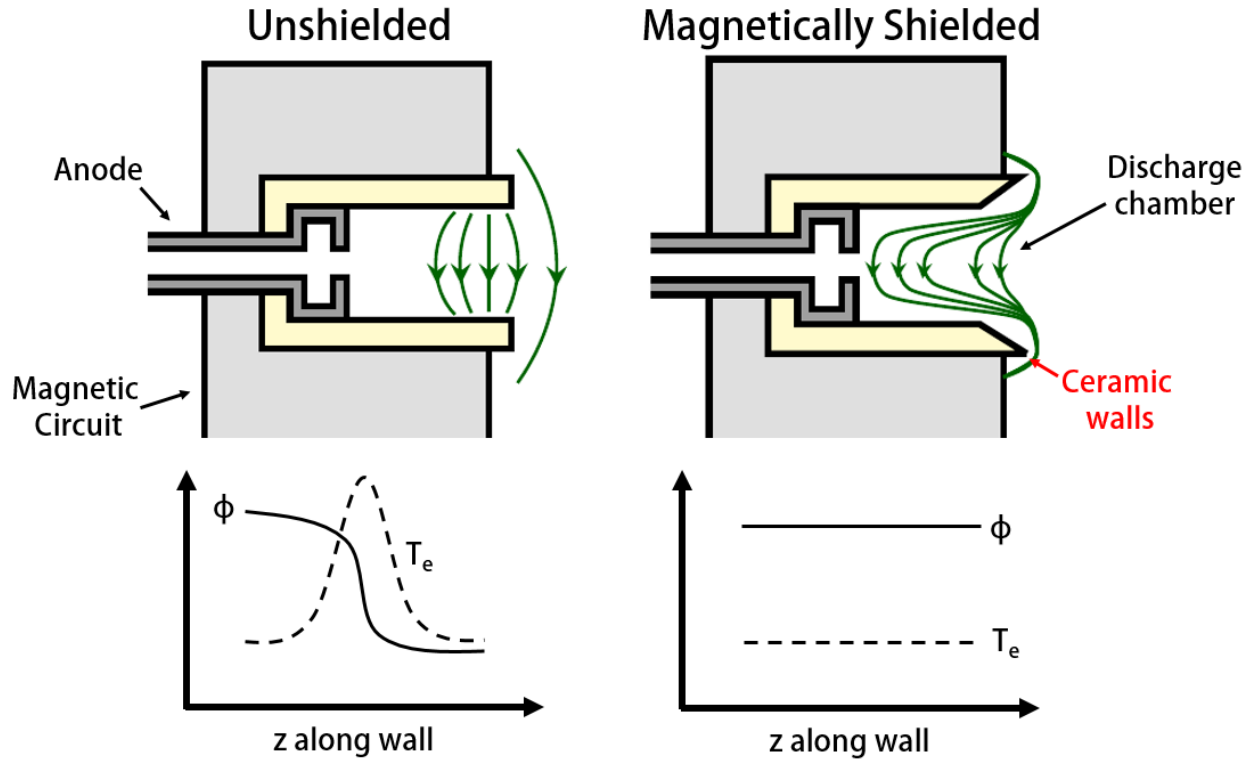


Fig. 1 Graphic depicting the differences between un-shielded and magnetically shielded Hall thrusters as well as the results electron temperature and plasma potential profiles along the wall.

that when electrons have a high mobility and low temperature (i.e. $T_e < 10$ eV), then there are only small changes in potential along the field line. This relation arises from Ohm's Law in the limit of low electron collisionality. This results in an electric field perpendicular to the magnetic-force-lines which accelerates ions away from the walls in addition to reducing the flux of ions to the walls. However, even ions that have low kinetic energy upon reaching the wall will still gain energy as they fall through the sheath potential. In order to consider this effect, we note that the sheath potential for boron nitride, the discharge chamber wall material, is dependent on the electron temperature and the secondary electron emission yield. Here, we follow the same process as Hofer et al.³ The secondary electron emission yield is given by²⁰

$$\gamma_e \approx \sigma_0 + (1 - \sigma_0) \frac{2T_e}{E_1}, \quad (4)$$

where σ_0 is the effective yield at zero energy and E_1 is the crossover energy. For boron nitride, the literature²⁰ gives values of 0.54 and 40 eV respectively. Assuming the sheath is not in the space charge limited regime (i.e. $T_e < 19.3$ eV), we can then calculate the resulting potential based on the one-dimensional equations from Hobbs and Wesson²¹ as adapted by Goebel and Katz as²²

$$\phi_s \approx -\frac{kT_e}{e} \ln \left[\sqrt{\frac{m_{Xe}}{8\pi m_e}} (1 - \gamma_e) \right]. \quad (5)$$

Since the wall sheath is proportional to the electron temperature, a very small sheath exists for low electron temperatures. Thus, should there be sufficiently cold electrons near the walls, the kinetic energy of ions towards the wall is significantly reduced and with it, the wall erosion is also reduced. The

erosion rate of the discharge channel is directly proportional to ion flux and the sputtering yield. This is also convolved with the incidence angle; however, for the purpose of this analysis we will assume all ions impact the wall perpendicularly. To define a metric for how much erosion occurs, we note that several works have suggested that ions as low as 30 eV can result in sputtering of wall materials.^{5,23,24}

As previously discussed, the erosion rate of the discharge chamber walls is dependent on the temperature of the grazing line. Equation 3 shows that if the electron temperature rises, then the plasma potential would decrease along the grazing line. This would then lead to a higher flux of ions towards the walls. Additionally, Eqn. 5 shows that increases in the electron temperature would also lead to an increase in the sheath potential magnitude. For instance, an increase from an electron temperature of 7 eV to 8 eV increases the sheath potential from -23.6 V to -26.3 V. Even though this is a very modest increase in temperature, the combined effects of the change in ion kinetic energy perpendicular to the walls with the increment in sheath potential could lead to ion impact energies above the sputtering threshold. However, it is challenging to predict what the influence of the shifting acceleration region due to neutral changes will be on the temperature of the grazing line. Thus, an experimental investigation of this effect is critical.

III. Experimental Apparatus

A. Thrusters

We used two thrusters for this investigation: the H9 and the N30. The H9 is a 9-kW single-channel magnetically shielded Hall thruster developed by NASA's Jet Propulsion Laboratory in collaboration with the University of Michigan and the Air Force Research Laboratory.²⁵ We operated the thruster at 4.5 kW of discharge power and 300 V of discharge current for this investigation which is well within its nominal operational power range of 4.5-9 kW. The thruster was operated in cathode tied configuration.²⁶ The N30 is a 33-kW two-channel magnetically shielded hall thruster developed by the University of Michigan in collaboration with the Jet Propulsion Laboratory.²⁷ The inner channel of this thruster shares geometry with the H9 Hall thruster. For this campaign, we operated in single-channel mode (inner channel only) at 4.5 kW and 300 V, again within the nominal operational range. For both thrusters, the same cathode design, with a nominal current up to 60 A, was used.²⁷ A picture of the setup can be seen in Fig. 2. The anode and cathodes were supplied with research-grade xenon through commercially available mass flow controllers. Power for the electromagnets and discharge was supplied with commercially available power supplies external to the chamber.

B. Facility

All testing occurred in the Large Vacuum Test Facility (LVTF) at the University of Michigan. LVTF is a 9 meter long, 6 meter diameter vacuum chamber with a base pressure of 0.1 μ Torr-Xe. Nominally, the chamber is pumped with five cryosails and thirteen LN₂-backed cryopumps. Pressure was measured using a Stabil Ion gauge located approximately 1 meter away from the thruster in line with the exit plane as seen in Figure 2. The gauge has a grounded mesh attached to the entrance per industry standard.²⁸ In order to vary the background pressure during testing, a combination of a reduced number of pumps and downstream gas injection was used. For the downstream gas injection, the flow was introduced approximately two meters away radially and one meter downstream of the thruster with the flow injected axially away from the thruster to ensure that neutrals did not preferentially go towards the thruster.

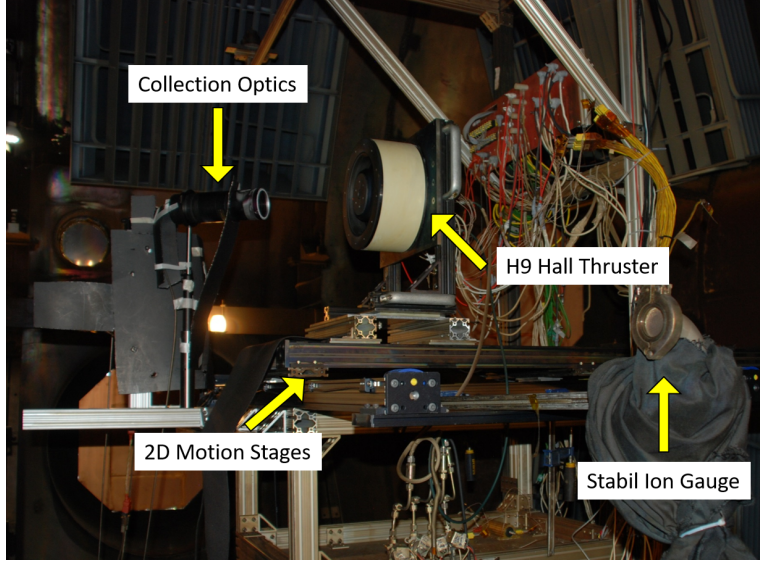


Fig. 2 The H9 Hall thruster setup for chamfer LIF. The thruster is mounted on two-dimensional motion stages to vary the interrogation point. The collection optics can be seen. One of the injection optics is outside of the picture and the other is blocked from view by the collection optics.

C. Diagnostics

In order to assess the centerline and near-wall ion velocity vectors, we employed a standard, multiplexed, non-resonant laser-induced fluorescence (LIF) scheme. We targeted the $5d_{7/2}^4 \rightarrow 6p_{5/2}^3$ metastable transition of xenon ions using a tunable diode laser with a taper amplifier. The interrogation volume, the intersection of the injection and collection optics, was approximately 1 mm^3 . Collected light was sent through a $\pm 4 \text{ nm}$ filter before being amplified through a photomultiplier tube and trans-impedance amplifier. Ultimately, this signal was measured with lock-in amplification. No corrections were made for Zeeman splitting, hyperfine structure, or broadening.

During testing, the optics were stationary and the thrusters were placed on radial-axial motion stages to vary the interrogation point. For each test point, we made three measurements: a channel centerline measurement of the acceleration region (axial velocity), a two-dimensional (parallel and perpendicular velocities) sweep along the inner chamfer, and a two-dimensional sweep along the outer chamfer. A notional diagram detailing the interrogation points is shown in Fig. 3. Ion velocity distribution functions were measured at six equally spaced points along the chamfer at two different axial distances away. In order to analyze the recorded data, we start by integral-normalizing the intensity to get the ion velocity distribution function (IVDF). For all the data, we fit a sum of Gaussians in order to reduce numerical noise in our calculations. An example of this fitting technique is seen in Fig. 4a. Additionally, for some traces, particularly on the inner chamfer, signal from the main ion beam was detected due to the orientation of the collection and injection optics. This only appeared in the perpendicular traces. In these cases, the Gaussian corresponding to this beam was subtracted from the trace. An example of a data set where this technique was performed is shown in Fig. 4b. Only the Gaussian associated with the chamfer data was integral-normalized. We then take the first moment of the distribution to calculate the mean as,

$$u_{mean} = \int_{u_1}^{u_2} u f(u) du \quad (6)$$

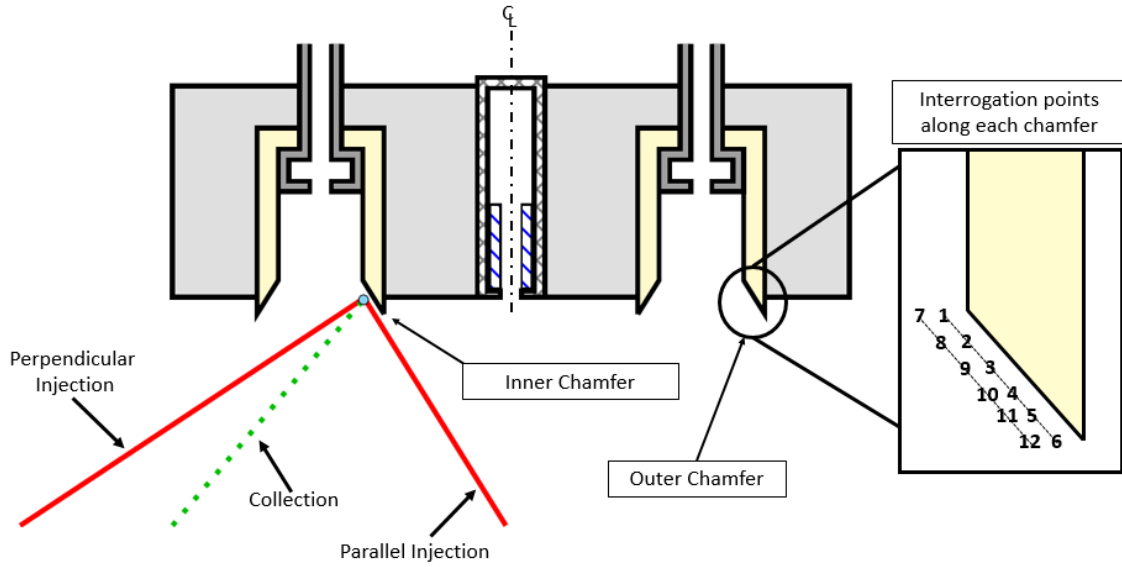


Fig. 3 Interrogation points along the chamfer to measured the ion velocity distribution functions.

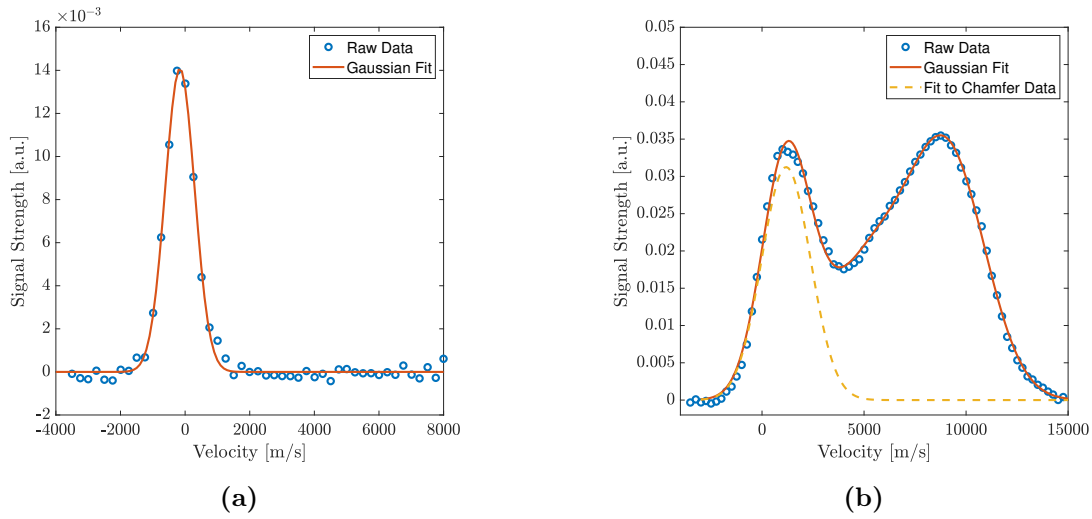


Fig. 4 Fitting technique for collected data. (a) An example of a single Gaussian fit used for the majority of the data. (b) An example of data where the main ion beam was detected. These data were fit with the sum of three Gaussians and the first Gaussian was taken as the true signal as the other two were associated with the main beam.

where u_1 and u_2 are the upper and lower bounds of velocity space, and $f(u)$ is the IVDF. For the centerline data, we then plot this mean velocity versus position to construct the “acceleration region.” For the chamfer data, we take the mean velocity in each direction to create a two-dimensional vector plot of ion trajectories.

D. Test Matrix

In order to study the impact of neutral density on the magnetic shielding of Hall thrusters, we performed studies at four operating conditions. For the H9, we operated at the base pressure ($4.8 \mu\text{Torr-Xe}$) well as an elevated background pressure ($15.8 \mu\text{Torr-Xe}$). For the N30, we operated the inner channel alone (at 4.5 kW) as well as the inner channel running (at 4.5 kW) with the outer channel nominal flow. The “nominal flow” for the outer channel is the flow for the equivalent condition on the outer channel: 300 V, 38.9 A. For all these test, the thrusters were operated at constant power and in cathode-tied configuration.

IV. Results

In this section, we first present the centerline profiles for each thruster. We then show the near-wall vector plots and detailed IVDF measurements for the H9. Next, we present the sheath analysis for the H9 before repeating all three of these results for the N30.

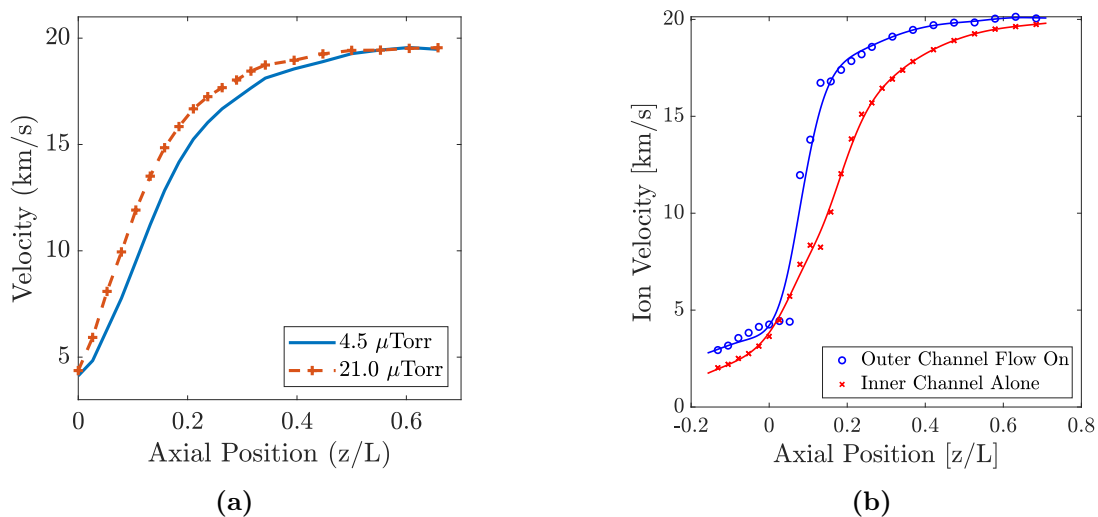


Fig. 5 Centerline profiles for both cases for the H9 (a) and the N30 (b).

To start, we plot the centerline profiles for each condition in Fig. 5. Figure 5a shows the acceleration region for both pressure cases for the H9 Hall thruster. We find that, as expected, there is an axial shift upstream of the acceleration with an increase in pressure and the overall shape of curve remains the same. Figure 5b shows the data, as well as fitted splines, for each condition of the N30 study. Similar to the H9, the plasma shifts axially inward when the outer channel flow is turned on. The magnitude of the shift is larger than the shift for the H9 with pressure. This is expected as the neutral density increase at the inner channel from neutrals emanating from the outer channel is much larger than the neutral density increase due to background pressure changes. Notably, it appears the shape of the acceleration region also changes with the introduction of neutrals from the outer channel. Studies on the X2, an unshielded two-channel Hall thruster, showed similar results.²⁹ While this result may be physical, we note that the oscillation strength increased significantly from 69.8% to 101.8% peak-to-peak of the mean current with the introduction of outer channel flow. Oscillations are known to widen measured velocity distributions which could lead to this change in perceived shape.^{16,30,31} Finally, due to the increase in oscillation strength, the signal-to-noise ratio decreased significantly. This could also be a contributing factor to the data shown in Fig. 5b. Regardless, both

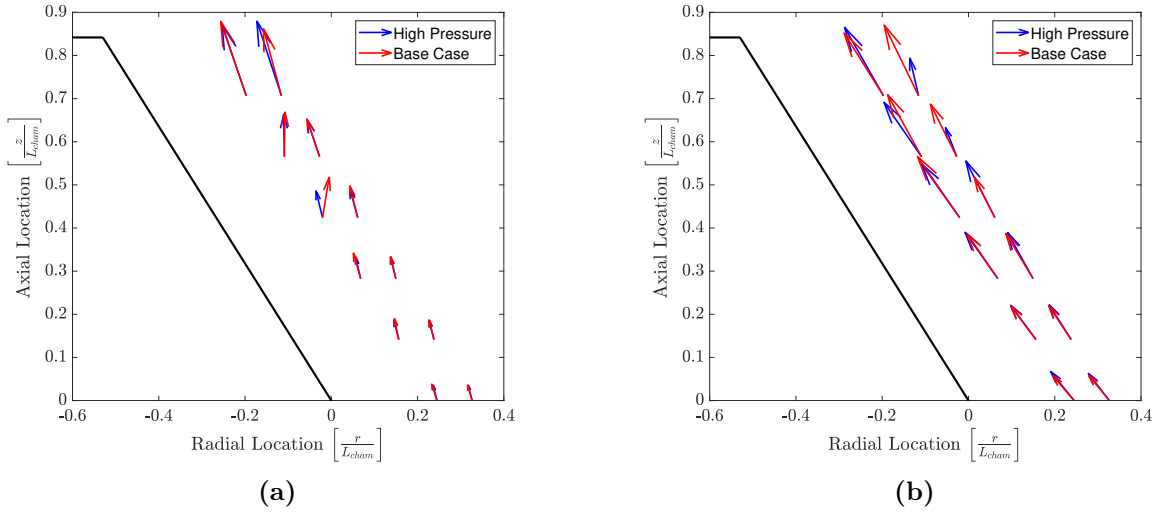


Fig. 6 Ion velocity vectors for both the base pressure case and the high pressure case along the inner (a) and outer (b) wall of the H9 Hall thruster.

centerline studies show the bulk plasma has shifted and thus, an investigation into how this shift impacts the near-wall ion velocities is warranted.

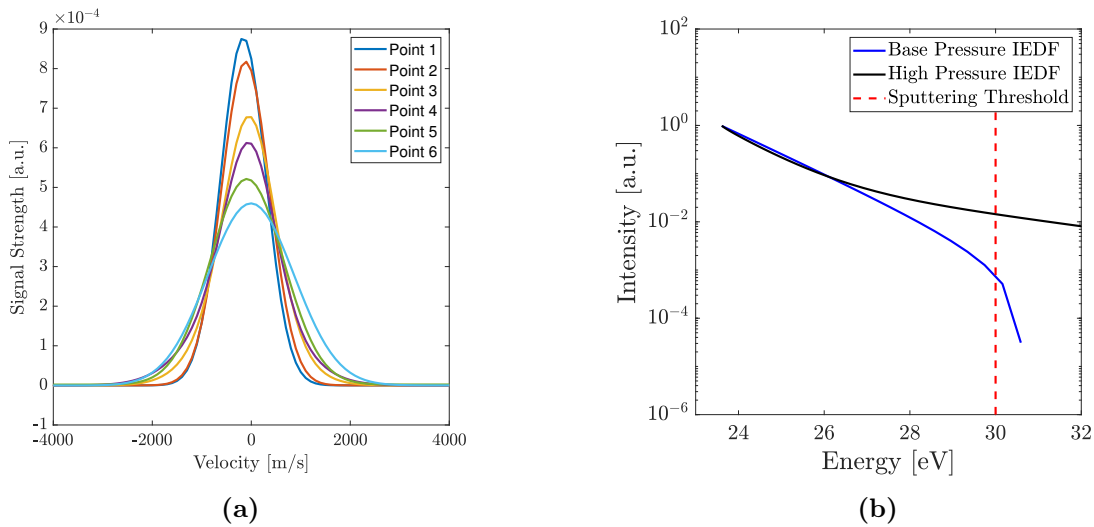


Fig. 7 Perpendicular VDFs along the outer channel wall (a) and (b) an analysis of the sheath for Point 6.

Figure 6 shows the vector plots (of the mean velocity) along both walls for each case of the H9. Overall, we see the profiles are qualitatively similar for both chamfers. Both chamfers show vectors that are expected, with the majority of the motion out of the channel and very little motion towards the wall. The outer wall of the H9 does show that in some locations, the vector has “turned” towards the wall at high pressure as compared to low pressure. This is expected with an increase in temperature of the grazing line. Regardless, the largest mean velocity towards the wall is 160 m/s. This corresponds to a very low directed energy and even with an electron temperature of 10 eV, the sheath

would still be sufficiently small (31 V) to eliminate erosion. However, we must also look at the width of the distribution, as an increase in the high velocity tail may contribute to enhanced erosion.

Figure 7a shows the perpendicular velocity distribution functions along the wall of the outer chamfer for the base pressure case of the H9, for points shown in Fig. 3. All points are a constant distance from the wall. We see that although Point 6 has one of the most positive average velocities, it also has the longest “tail” in the negative (toward the wall) velocity space. This was also true for the high pressure case. Thus, in order to perform a sheath analysis, we look at Point 6 for both cases. We convert the negative velocity portion of the VDF for each case to an ion energy distribution function (IEDF) and then accelerate it through a sheath corresponding to an electron temperature of 7 eV. This temperature was chosen based on results from the H6MS studies.³ The results of this analysis are seen in Fig. 7b. While the majority of the ions are below the sputtering threshold, we do see that at higher pressures, a larger fraction (from 0.1% to 4.0%) have sufficient energy to sputter the wall. Thus, while very subtle, we would expect the erosion rate to be higher for the high pressure case than the low pressure case.

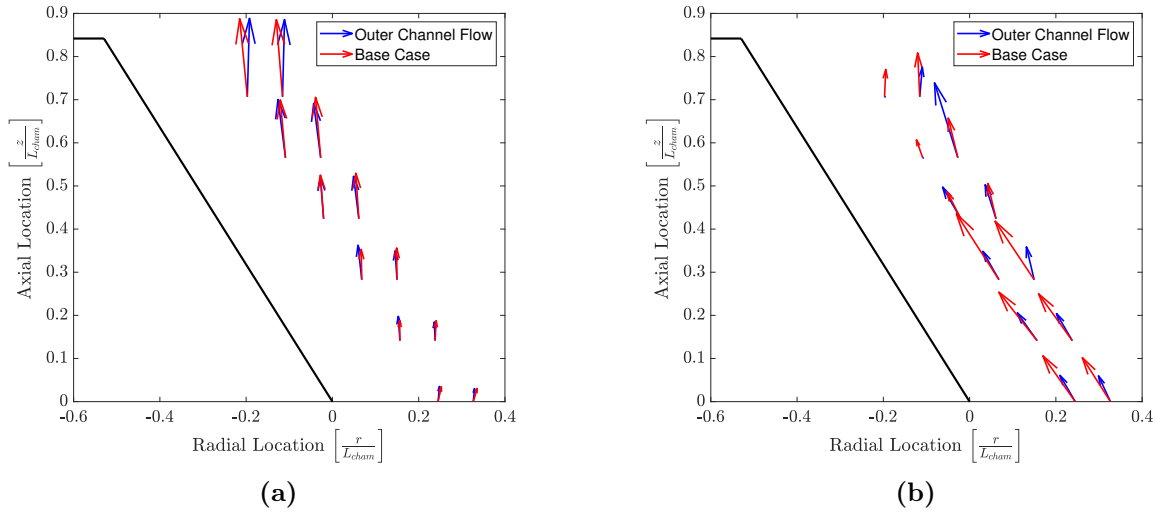


Fig. 8 Ion velocity vectors for both the base pressure case and the high pressure case along the inner (a) and outer (b) wall of the N30.

Next, we look at the N30 results. The two-dimensional vector plots for both the inner and outer chamfers are seen in Fig. 8. Unfortunately, due to signal-to-noise issues for the outer flow case, we were unable to resolve points 5 and 6 for the outer chamfer. Overall, we see the results are very similar to the H9 study. There does not appear to be any major changes to the velocity vectors near the wall. The outer wall does seem to show that the average parallel velocity is lower when flowing through the outer channel than when just firing the inner channel.

Finally, we look at the actual VDFs, and the corresponding sheath analysis. Due to the missing data at Point 6, and based on the results shown in Fig. 9a, we chose to analyze Point 1 for the N30. These results are seen in Figure 9b. Surprisingly, there does not appear to be a significant difference between the two traces. This could be indicative that changes in the plasma behavior (for instance, oscillations) are affecting the near wall ion trajectories. Alternatively, we consider that the acceleration region did not actually shift and was instead just compressed, as the results suggested.

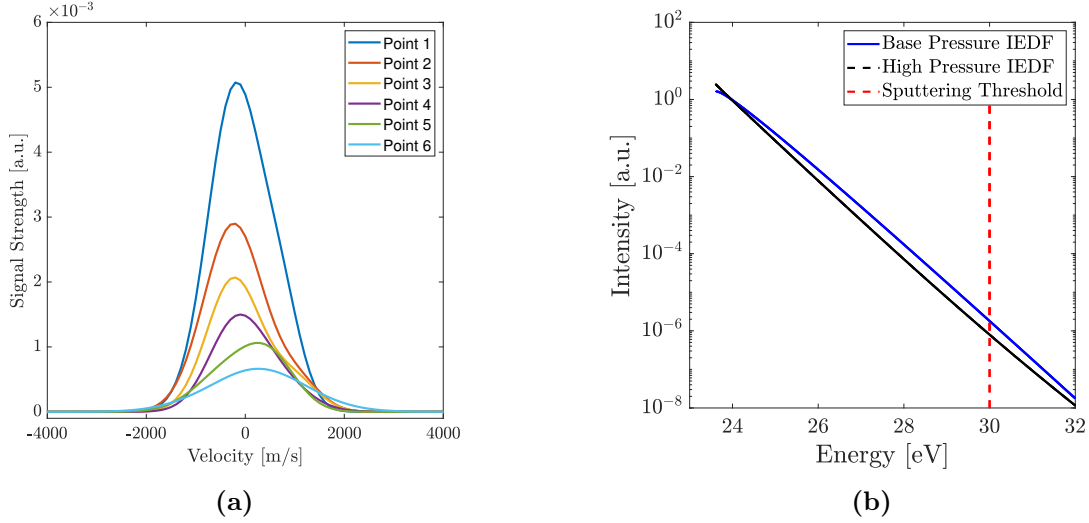


Fig. 9 Perpendicular VDFs along the outer channel wall (a) and (b) an analysis of the sheath for Point 1 for the N30.

If this was true, while the downstream ion velocity profile (as well as potential and electron temperature) profiles would change, the upstream profile would not change. Thus, the grazing line would be intersecting the centerline at the same electron temperature in both cases. This would suggest that no change in ion wall trajectories would be expected as the results show.

V. Discussion

In this study, we showed the result of changing the local neutral density on the shielding of magnetically shielded Hall thrusters. In general, we find that the impacts are small and likely do not have a large impact on lifetime. The study on the H9 tells us that higher pressures will likely lead to slightly higher erosion rates due to a larger fraction of ions above the sputtering limit. However, this behavior would actually correlate to a longer lifetime in space than on the ground as pressure decreases between the two locations. If the plasma is moved downstream, like in flight, the grazing lines may be sampling even colder plasma. This typically leads to higher divergence, which could alter the trajectories beyond the measurements we presented here. This is important for other thruster parameters, such as performance and pole erosion, as well as spacecraft interactions. While the ion trajectories are not changing substantially, a slight increase in the electron temperature (from say 7 to 8 eV) would result in a larger sheath potential. In turn, this could accelerate a much larger portion of the ions to above the sputtering threshold. We did not attempt to characterize this temperature during this study; however, based on our results, we do not believe this temperature is changing significantly. Because the ion trajectories, as well as the magnitude of the mean velocity in each direction, does not change substantially between conditions, we argue that this implies there are no substantial changes to the electron temperature of the grazing line.

For the NHT, we do not see any major impacts on the IEDF or the ion trajectories. We do note that the lack of data at Points 5 and 6 do present an incomplete picture. We believe the large change in oscillatory behavior between the two cases is the reason for both the lack of signal-to-noise at the outer flow case and the lack of a clear trend for the study. Ideally, this study would be repeated with the outer channel plasma on, as without the plasma, the neutral density is higher than would be expected in dual-channel mode. This may have contributed to the change in oscillation behavior.

Overall, this study indicates that the erosion profile of the thruster is not dependent on firing configuration. This conclusion would be strengthened with wall electron temperature measurements which could indicate whether these subtle changes are impacting the overall sheath potential, and therefore, erosion.

With decreasing pressure, the acceleration region moves outward. This is a well documented phenomenon throughout literature.^{15,16,32} This, in turn, typically decreases performance. Previous studies have suggested that running the cathode flow rich can “push” this acceleration region inwards to recover any lost performance.³³ However, there did exist a risk for magnetically shielded thrusters that this would lead to higher erosion if the location was not precisely controlled. This study indicates that this is not a large concern as the shifts in the plasma location here did not drastically alter the near-wall behavior.

VI. Conclusion

We presented a study into the impact of neutral density on the magnetic shielding of Hall thrusters. To accomplish this, we first probed the near-wall ion velocity distributions of the H9 Hall thruster at low and high pressure. We then measured these profiles on the inner channel of the N30 with and without outer channel flow. The centerline profiles indicated that the bulk plasma was indeed shifting as the neutral density changed. Near-wall velocity vector plots showed that for both the N30 and the H9, there were only slight changes in the ion trajectories between the cases. For the H9, a sheath analysis showed that higher erosion was expected with increasing pressure; however, the majority (96%) of the plasma remained below the sputtering limit. For the N30, the tail of the distribution did not change noticeably and no change in erosion is expected. Combined, these results indicate that while neutral density will change the bulk plasma significantly, the near-wall behavior of the ions is not affected by this movement.

Acknowledgments

The authors would like to acknowledge Marcel Georgin, Ethan Dale, and Matt Byrne for their help during LIF setup as well as the entirety of the Plasmadynamics and Electric Propulsion Laboratory for their assistance with the experiment. The authors would also like to acknowledge funding provided by NASA Space Technology Research Fellowship grant number NNX15AQ43H. This work also was supported by an AFOSR grant from the Space Propulsion and Power portfolio.

References

- [1] Hofer, R., Goebel, D., Mikellides, I., and Katz, I., “Design of a laboratory Hall thruster with magnetically shielded channel walls, phase II: Experiments,” *48th AIAA/ASME/SAE/ASEE Joint Propulsion Conference & Exhibit*, 2012, p. 3788.
- [2] Hofer, R. R., Jorns, B. A., Polk, J. E., Mikellides, I. G., and Snyder, J. S., “Wear test of a magnetically shielded Hall thruster at 3000 seconds specific impulse,” *33rd International Electric Propulsion Conference*, 2013, pp. 1–24.
- [3] Hofer, R. R., Goebel, D. M., Mikellides, I. G., and Katz, I., “Magnetic shielding of a laboratory Hall thruster. II. Experiments,” *Journal of Applied Physics*, Vol. 115, No. 4, 2014, pp. 043304.
- [4] Mikellides, I. G., Katz, I., Hofer, R. R., Goebel, D. M., De Grys, K., and Mathers, A., “Magnetic shielding of the channel walls in a Hall plasma accelerator,” *Physics of Plasmas*, Vol. 18, No. 3, 2011, pp. 033501.
- [5] Mikellides, I. G., Katz, I., Hofer, R. R., and Goebel, D. M., “Magnetic shielding of walls from the unmagnetized ion beam in a Hall thruster,” *Applied Physics Letters*, Vol. 102, No. 2, 2013, pp. 023509.

- [6] Mikellides, I. G., Katz, I., Hofer, R. R., and Goebel, D. M., “Magnetic shielding of a laboratory Hall thruster. I. Theory and validation,” *Journal of Applied Physics*, Vol. 115, No. 4, 2014.
- [7] Sekerak, M., Hofer, R., Polk, J., Jorns, B., and Mikellides, I., “Wear testing of a magnetically shielded hall thruster at 2000 s specific impulse,” *34th International Electric Propulsion Conference, IEPC-2015-155, Kobe, Japan*, 2015.
- [8] Grimaud, L. and Mazouffre, S., “Performance comparison between standard and magnetically shielded 200 W Hall thrusters with BN-SiO₂ and graphite channel walls,” *Vacuum*, Vol. 155, 2018, pp. 514–523.
- [9] Jorns, B. A. and Hofer, R. R., “Plasma oscillations in a 6-kW magnetically shielded Hall thruster,” *Physics of Plasmas*, Vol. 21, No. 5, 2014, pp. 053512.
- [10] Jorns, B. A. and Hofer, R. R., “Low frequency plasma oscillations in a 6-kW magnetically shielded hall thruster,” *49th AIAA/ASME/SAE/ASEE Joint Propulsion Conference*, 2013, p. 4119.
- [11] Kamhawi, H., Haag, T., Huang, W., Yim, J., Herman, D. A., Peterson, P. Y., Williams, G., Gilland, J., Hofer, R. R., and Mikellides, I. G., “Performance, Facility Pressure Effects, and Stability Characterization Tests of NASA’s 12.5-kW Hall Effect Rocket with Magnetic Shielding Thruster,” *52nd AIAA/SAE/ASEE Joint Propulsion Conference*, 2016, p. 4826.
- [12] Polk, J. E., Lobbia, R., Barriault, A., Guerrero, P., Mikellides, I., and Ortega, A. L., “Inner Front Pole Cover Erosion in the 12.5 kW HERMeS Hall Thruster Over a Range of Operating Conditions,” *35th International Electric Propulsion Conference, IEPC Paper*, Vol. 409, 2017.
- [13] Jorns, B., Dodson, C. A., Anderson, J. R., Goebel, D. M., Hofer, R. R., Sekerak, M. J., Lopez Ortega, A., and Mikellides, I. G., “Mechanisms for pole piece erosion in a 6-kW magnetically-shielded Hall thruster,” *52nd AIAA/SAE/ASEE Joint Propulsion Conference*, 2016, p. 4839.
- [14] Hofer, R. R. and Anderson, J. R., “Finite pressure effects in magnetically shielded Hall thrusters,” *50th AIAA/ASME/SAE/ASEE Joint Propulsion Conference*, 2014, p. 3709.
- [15] Cusson, S. E., Dale, E. T., Jorns, B. A., and Gallimore, A. D., “Acceleration region dynamics in a magnetically shielded Hall thruster,” *Physics of Plasmas*, Vol. 26, No. 2, 2019, pp. 023506.
- [16] Nakles, M. R. and Hargus, W. A., “Background pressure effects on ion velocity distribution within a medium-power Hall thruster,” *Journal of Propulsion and Power*, Vol. 27, No. 4, 2011, pp. 737–743.
- [17] Chaplin, V. H., Conversano, R. W., Lobbia, R. B., Ortega, A. L., Mikellides, I. G., Hofer, R. R., and Jorns, B. A., “Laser-Induced Fluorescence Measurements of the Acceleration Zone in the 12.5 kW HERMeS Hall Thruster,” *35th International Electric Propulsion Conference*, Vol. 229, 2017, pp. 8–12.
- [18] Jackson, J., Allen, M., Myers, R., Hoskins, A., Soendker, E., Welander, B., Tolentino, A., Hablitzel, S., Hall, S., Gallimore, A., et al., “100 kW Nested Hall Thruster System Development,” 2017.
- [19] Cusson, S. E., Georgin, M. P., Dragnea, H. C., Dale, E. T., Dhaliwal, V., Boyd, I. D., and Gallimore, A. D., “On channel interactions in nested Hall thrusters,” *Journal of Applied Physics*, Vol. 123, No. 13, 2018, pp. 133303.
- [20] Dunaevsky, A., Raitses, Y., and Fisch, N. J., “Secondary electron emission from dielectric materials of a Hall thruster with segmented electrodes,” *Physics of Plasmas*, Vol. 10, No. 6, 2003, pp. 2574–2577.
- [21] Hobbs, G. and Wesson, J., “Heat flow through a Langmuir sheath in the presence of electron emission,” *Plasma Physics*, Vol. 9, No. 1, 1967, pp. 85.
- [22] Goebel, D. M. and Katz, I., *Fundamentals of electric propulsion: ion and Hall thrusters*, Vol. 1, John Wiley & Sons, 2008.

- [23] Garnier, Y., Viel, V., Roussel, J.-F., and Bernard, J., “Low-energy xenon ion sputtering of ceramics investigated for stationary plasma thrusters,” *Journal of Vacuum Science & Technology A: Vacuum, Surfaces, and Films*, Vol. 17, No. 6, 1999, pp. 3246–3254.
- [24] Garrigues, L., Hagelaar, G., Bareilles, J., Boniface, C., and Boeuf, J., “Model study of the influence of the magnetic field configuration on the performance and lifetime of a Hall thruster,” *Physics of Plasmas*, Vol. 10, No. 12, 2003, pp. 4886–4892.
- [25] Hofer, R. R., Cusson, S. E., Lobbia, R. B., and Gallimore, A. D., “The H9 Magnetically Shielded Hall Thruster,” *35th International Electric Propulsion Conference*, 2017.
- [26] Hofer, R. R., Jorns, B. A., Katz, I., and Brophy, J. R., “Hall effect thruster electrical configuration,” Oct. 5 2017, US Patent App. 15/474,480.
- [27] Cusson, S. E., Hofer, R. R., Georgin, M. G., Vazsonyi, A. R., Jorns, B. A., and Gallimore, A. D., “A 30-kW Class Magnetically Shielded Nested Hall Thruster,” *36th International Electric Propulsion Conference*, 2019 (Submitted).
- [28] Dankanich, J. W., Walker, M., Swiatek, M. W., and Yim, J. T., “Recommended practice for pressure measurement and calculation of effective pumping speed in electric propulsion testing,” *Journal of Propulsion and Power*, Vol. 33, No. 3, 2016, pp. 668–680.
- [29] Georgin, M. P., Dhaliwal, V., and Gallimore, A., “Investigation of channel interactions in a nested Hall thruster part i: Acceleration region velocimetry,” *52nd AIAA/SAE/ASEE Joint Propulsion Conference*, 2016, p. 5030.
- [30] Mazouffre, S. and Bourgeois, G., “Spatio-temporal characteristics of ion velocity in a Hall thruster discharge,” *Plasma Sources Science and Technology*, Vol. 19, No. 6, 2010, pp. 065018.
- [31] Hargus, W., Nakles, M., Tedrake, R., and Pote, B., “Effect of Anode Current Fluctuations on Ion Energy Distributions within a 600 W Hall Effect Thruster,” *44th AIAA/ASME/SAE/ASEE Joint Propulsion Conference & Exhibit*, 2008, p. 4724.
- [32] MacDonald-Tenenbaum, N., Pratt, Q., Nakles, M., Pilgram, N., Holmes, M., and Hargus Jr, W., “Background Pressure Effects on Ion Velocity Distributions in an SPT-100 Hall Thruster,” *Journal of Propulsion and Power*, Vol. 35, No. 2, 2019, pp. 403–412.
- [33] Cusson, S. E., Byrne, M., Jorns, B., and Gallimore, A., “Investigation into the Use of Cathode Flow Fraction to Mitigate Pressure-Related Facility Effects on a Magnetically Shielded Hall Thruster,” *AIAA Propulsion and Energy 2019 Forum*, 2019, p. 4077.